

Vortex solitons in two-dimensional spin-orbit coupled Bose-Einstein condensates: effects of the Rashba-Dresselhaus coupling and the Zeeman splitting

Hidetsugu Sakaguchi

*Department of Applied Science for Electronics and Materials,
Interdisciplinary Graduate School of Engineering Sciences,
Kyushu University, Kasuga, Fukuoka 816-8580, Japan*

E. Ya. Sherman

*Department of Physical Chemistry, University of the Basque Country UPV-EHU, 48940, Bilbao, Spain and
IKERBASQUE, Basque Foundation for Science, Bilbao, Spain*

Boris A. Malomed

*Department of Physical Electronics, School of Electrical Engineering,
Faculty of Engineering, Tel Aviv University, Tel Aviv 69978, Israel*

(Dated: September 24, 2018)

We present an analysis of two-dimensional (2D) matter-wave solitons, governed by the pseudo-spinor system of Gross-Pitaevskii equations with self- and cross-attraction, which includes the spin-orbit coupling (SOC) in the general Rashba-Dresselhaus form, and, separately, the Rashba coupling and the Zeeman splitting. Families of semi-vortex (SV) and mixed-mode (MM) solitons are constructed, which exist and are stable in free space, as the SOC terms prevent the onset of the critical collapse and create the otherwise missing ground states in the form of the solitons. The Dresselhaus SOC produces a destructive effect on the vortex solitons, while the Zeeman term tends to convert the MM states into the SV ones, which eventually suffer delocalization. Existence domains and stability boundaries are identified for the soliton families. For physically relevant parameters of the SOC system, the number of atoms in the 2D solitons is limited by $\sim 1.5 \times 10^4$. The results are obtained by means of combined analytical and numerical methods.

PACS numbers: 03.75.Mn, 03.75.Lm, 72.25.-b, 05.45.Yv

I. INTRODUCTION.

Recent developments in producing macroscopic ensembles of cold atoms have greatly extended an experimentally accessible variety of quantum phenomena in systems of interacting particles, with both repulsion and attraction between them. Bosonic gases can be optically cooled down to the temperature of the Bose-Einstein condensation (BEC) [1, 2]. Properties of these condensates, including the strength and sign of inter-atomic interactions, can be controlled by means of the Feshbach resonance [3], which provides a powerful tool for the creation and control of various phases in the ultracold gases.

Recently, a great deal of interest has been drawn to the experimentally demonstrated [4] ability of binary BEC to emulate the spin-orbit coupling (SOC) and Zeeman effect, which play a fundamentally important role in the solid-state physics. Both types of the SOC known in terms of the solids, which are represented by the Dresselhaus [5] and Rashba [6] Hamiltonians, can be simulated in BEC, along with the Zeeman splitting [7]. Basic results produced by recent research in this field have been summarized in reviews [8, 9]. Although the true spin of bosonic atoms, such as ^{87}Rb , used in these experiments, is zero, the (pseudo)spinor wave function of the binary condensate has two components, which enables the use of the corresponding *pseudospin* 1/2 for emulating the quantum dynamics of fermionic carriers in solids

by means of the bosonic gases. A majority of experimental works on the SOC [9] were dealing with effectively one-dimensional (1D) settings. Recently, the realization of the SOC in the two-dimensional (2D) geometry was reported [10, 11], which suggests further theoretical analysis of the 2D settings.

While the (pseudo) SOC in BEC is represented by the linear interaction between two spatially inhomogeneous components of the condensate (as it must be, because it emulates the effects from linear quantum mechanics), see Eqs. (2) and (3) below, the interplay of this linear coupling with the mean-field nonlinearity of the BEC gives rise to diverse nonlinear phenomena, such as 1D solitons [12], 2D gap solitons [13], stripe phases [14], and many others [15]. Further, it is well known that BEC can form vortex structures [16, 17]. Naturally, matter-wave patterns in the form of single vortices and vortex lattices are nontrivially affected by the SOC [18]. In particular, these works have demonstrated that specific to the SOC system are 2D composite states in the form of *half-vortices* (we call them *semi-vortices* (SVs) below, following Ref. [19]), in which one component carries vorticity $S = \pm 1$, while the other one has $S = 0$. The SOC also plays an important role in the formation of three-dimensional (3D) BEC structures [20], including complex topologically organized modes, such as skyrmions [21].

A majority of the above-mentioned works, except for those which were dealing with 1D bright solitons [12],

addressed the binary BEC with the self-repulsive intrinsic nonlinearity, and cross-repulsion between two components of the pseudo-spinor wave function. In the case of self-attraction, a commonly known problem is that 2D and 3D fundamental (zero-vorticity) solitons, supported by cubic terms, are strongly unstable in the free space, due to the occurrence of the critical and supercritical *wave collapse* in the same 2D and 3D settings, respectively [22], while vortical solitons are subject to a still stronger splitting instability [23]. In particular, in the 2D case, the Gross-Pitaevskii/nonlinear Schrödinger equation (GPE/NLSE) with the cubic self-attraction term gives rise to *degenerate* families of fundamental *Townes solitons* with $S = 0$ [24] and their vortical counterparts with $S \geq 1$ [25]. The degeneracy means that the entire family has a single value of the norm [see Eq. (9) below], which is, as a matter of fact, the value separating collapsing and decaying solutions, hence the Townes solitons, that play the role of separatrices between these two types of the dynamical behavior, are themselves completely unstable. In turn, the degeneracy is a consequence of the specific scale invariance of the GPE/NLSE in two dimensions.

An unexpected result, which opens novel perspectives for the use of the SOC in BEC, was recently reported in Ref. [19] (see also an extension of the analysis in Refs. [26, 27]): the linear SOC terms of the Rashba type [6] stabilize 2D free-space solitons, in the form of the above-mentioned semi-vortices, with $S = 0$ and $S = \pm 1$ in the two components, or in the form of *mixed modes* (MMs), i.e., soliton complexes with combinations of terms carrying $S = 0$ and $S = +1$ in one component, and $S = 0$, $S = -1$ in the other. The explanation to this benign effect of the SOC is that this coupling is characterized by an additional length parameter, that is the spin precession length (typically, of the order of few micron [4, 7–9]), inversely proportional to the SOC strength. Thus, the SOC defines a specific length scale in the system, thus breaking the above-mentioned scale invariance, lifting the norm degeneracy of the solitons, and eventually pushing their norm *below* the threshold necessary for the onset of the collapse. Being protected against the collapse, the SV and MM solitons enjoy stabilization and actually introduce a ground state (GS), which is missing in the scale-invariant 2D GPE/NLSE with the self-attraction [19]. The aptitude of the SOC terms in 2D to suppress the immediate onset of the critical collapse was also demonstrated in other contexts (unrelated to solitons) in Refs. [28] and [29]. The stabilization of 2D solitons in free space is a possibility of obvious interest to many nonlinear systems beyond the limits of the studies of cold gases. In particular, it has been demonstrated that 2D spatiotemporal solitons can be stabilized by means of a similar mechanism in an optics setting, based on a planar dual-core nonlinear waveguide with temporal dispersion of the linear coupling between the cores [30].

In 3D, the supercritical collapse cannot be suppressed

by the SOC terms. Nevertheless, recent work [31] has demonstrated that the interplay of the linear SOC interactions and the cubic self- and cross-attraction gives rise to two-component 3D solitons of the same two generic types, SVs and MMs, which are metastable states. Although they cannot be protected against falling into the supercritical collapse, if subjected to sudden strong compression, these self-trapped modes are completely stable against small perturbations.

The stability of the 2D SV and MM solitons was established in Refs. [19, 26, 27] for the SOC of the Rashba type, acting in the combination with the cubic self-attraction, and cross-attraction between the two components of the binary BEC. Because a physically relevant generic situation includes a combination of the Rashba and Dresselhaus SOC [7], and the stability of the 2D solitons in free space is quite an unexpected result, it is relevant to extend the analysis to the full Rashba-Dresselhaus Hamiltonian, which is one of major objectives of the present work. This analysis is performed in Section 2, a general conclusion being that the addition of the Dresselhaus interaction leads to shrinkage of the existence regions for stable 2D solitons, eventually leading to onset of delocalization. The analysis establishes the existence boundaries of the SV and MM solitons in the case of the combined Rashba-Dresselhaus interaction.

Another objective of this work is to consider effects of the Zeeman splitting on the 2D solitons, which is an obviously relevant problem too, in terms of both the emulation of the solid-state physics and the BEC dynamics per se. This problem is addressed by means of combined analytical and numerical methods, including a variational approximation (VA), in Section 3, where it is shown that the increase in the Zeeman terms leads to a transition from the MM solitons to their SV counterparts, and, eventually, to delocalization. The paper is concluded by Section 4.

II. COMBINED EFFECTS OF THE RASHBA AND DRESSELHAUS SPIN-ORBIT COUPLINGS ON 2D SOLITONS

A. The model and classification of the states

We begin with the consideration of the action of the synthetic SOC, including both the Rashba and the Dresselhaus terms, in the 2D space, (x, y) . In the mean-field approximation [2], the pseudo-spinor condensate is described by a two-component wave function [8, 9], $[\phi_+, \phi_-]^T$, with norm

$$N = \iint (|\phi_+|^2 + |\phi_-|^2) dx dy, \quad (1)$$

which is proportional to the total number of atoms in the binary BEC. The applicability of this approach to SOC settings was demonstrated in many works [8, 9, 32],

including the case of attractive interactions [33]. Accordingly, the evolution of the wave function is governed by the system of coupled GPEs, written here in the scaled form [4, 8, 9]:

$$i\frac{\partial\phi_+}{\partial t} = -\frac{1}{2}\nabla^2\phi_+ - (|\phi_+|^2 + \gamma|\phi_-|^2)\phi_+ + \left(\lambda\widehat{D}^{[-]}\phi_- - i\lambda_D\widehat{D}^{[+]}\phi_-\right), \quad (2)$$

$$i\frac{\partial\phi_-}{\partial t} = -\frac{1}{2}\nabla^2\phi_- - (|\phi_-|^2 + \gamma|\phi_+|^2)\phi_- - \left(\lambda\widehat{D}^{[+]}\phi_+ + i\lambda_D\widehat{D}^{[-]}\phi_+\right), \quad (3)$$

where λ and λ_D are constants of the Rashba and Dresselhaus SOC ($\lambda \equiv 1$ is fixed below by means of rescaling [34]), the nonlinear interactions are assumed to be attractive, γ being the relative strength of the cross-attraction between the two components, while the self-attraction coefficients are scaled to be 1, and we introduced operators $\widehat{D}^{[\pm]} \equiv \partial/\partial x \pm i\partial/\partial y$. As for parameter γ , it may be adjusted, if necessary by means of the Feshbach resonance. The applicability of this technique to the BEC under the action of the SOC was recently analyzed in Ref. [35], see also review [8].

The comparison of scaled 2D equations (2) and (3) with the underlying system of 3D GPEs presented in the physical units readily shows that the unit length in these equations corresponds to the spatial scale about $1 \mu\text{m}$. Further, by assuming typical values of the transverse confinement length $\simeq 3 \mu\text{m}$ and the scattering length $\sim -0.1 \text{ nm}$ describing the interatomic attraction, we find that $N = 1$ in the present notation is tantamount to $\simeq 3,000$ atoms.

The spectrum of plane waves generated by the linearized version of Eqs. (2), (3), $\phi_{\pm} \sim \exp(i(\mathbf{k} \cdot \mathbf{r}) - i\epsilon t)$, where \mathbf{k} is the wave vector, contains two branches,

$$\epsilon_{\pm} = \frac{k^2}{2} \pm \sqrt{(1 + \lambda_D^2)k^2 + 4\lambda_D k_x k_y}. \quad (4)$$

Note that the spectrum is anisotropic in the presence of the Dresselhaus coupling, $\lambda_D \neq 0$. The anisotropy, even if relatively weak, qualitatively alters the vortex solitons, and eventually causes their delocalization, as shown below.

In the absence of the Dresselhaus coupling, 2D self-trapped states (solitons) of two different types, SVs and MMs, were obtained as stationary solutions of Eqs. (2),(3) in Refs. [19] and [26]. Imaginary-time simulations, as well as an analytical variational approximation, produced these solutions starting from the Gaussian *ansätze* written in terms of the polar coordinates, (r, θ) :

$$\begin{aligned} (\phi_+)_{\text{SV}} &= A_1 e^{-\alpha_1 r^2 - i\mu t}, \\ (\phi_-)_{\text{SV}} &= A_2 r e^{i\theta} e^{-\alpha_2 r^2 - i\mu t}, \end{aligned} \quad (5)$$

$$\begin{aligned} (\phi_+)_{\text{MM}} &= B_1 e^{-\beta_1 r^2 - i\mu t} - B_2 r e^{-i\theta} e^{-\beta_2 r^2 - i\mu t}, \\ (\phi_-)_{\text{MM}} &= B_1 e^{-\beta_1 r^2 - i\mu t} + B_2 r e^{i\theta} e^{-\beta_2 r^2 - i\mu t}, \end{aligned} \quad (6)$$

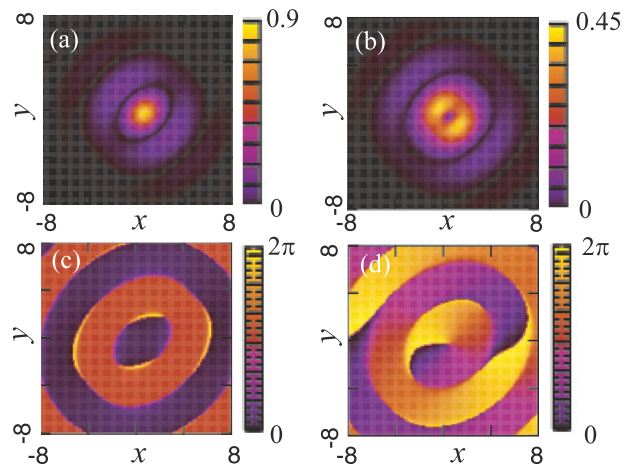


FIG. 1: Plots of (a) $|\phi_+(x, y)|$, (b) $|\phi_-(x, y)|$, (c) phase of $\phi_+(x, y)$, and (d) phase of $\phi_-(x, y)$ for a semi-vortex soliton at $\lambda_D = 0.05$, $\gamma = 0.9$, and $N = 3.5$. It is worth mentioning that strong deformation of the semi-vortex components along the $x = \pm y$ directions can be anticipated from Eq. (4), showing a strong change in the spectrum at $k_x = \pm k_y$.

where μ is the chemical potential, factors $\exp(\pm i\theta)$ carry vorticities $S = \pm 1$, while constants $A_{1,2}$, $B_{1,2}$ and $\alpha_{1,2}^{-1/2}$, $\beta_{1,2}^{-1/2}$ represent the amplitudes and widths of the input.

In the case of $\lambda_D = 0$, the so obtained SV and MM modes are stable and produce the system's GS, severally, at $\gamma < 1$ and $\gamma > 1$. Precisely at $\gamma = 1$, both types are stable and, moreover, they are embedded into a broader family with an extra free parameter (existing solely at $\gamma = 1$), which makes it possible to link the SV and MM modes [26].

B. Semi-vortices and mixed-mode states

In the presence of the Dresselhaus terms, we have found the GS of system (2), (3) by means of the imaginary-time simulations. We start with small $\lambda_D = 0.05$, and, in particular, focus on the distinction between the cases of $\gamma < 1$ and $\gamma > 1$, as they produce different types of the GS in the absence of the Dresselhaus terms [19]. The results demonstrate that stationary solutions keep the same vorticity structure which is assumed in initial *ansätze* (5) and (6).

Figures 1(a) and (b) display plots of $|\phi_+(x, y)|$ and $|\phi_-(x, y)|$ and Figs. 1(c) and (d) are plots of phases of $\phi_+(x, y)$ and $\phi_-(x, y)$ for an SV state, at $\lambda_D = 0.05$ and $\gamma = 0.9$. Similarly, Figure 2 shows moduli and phases of $\phi_+(x, y)$ and $\phi_-(x, y)$ for a MM state at $\lambda_D = 0.05$ and $\gamma = 1.1$. The well-defined vorticity for ϕ_- is shown in Fig. 1 (d), while the phase of the mixed-state structure of ϕ_+ and ϕ_- , as shown in Figs. 2(c) and (d), is more complicated. In terms of spectrum (4), the term accounting for the distortion of the shape of the density

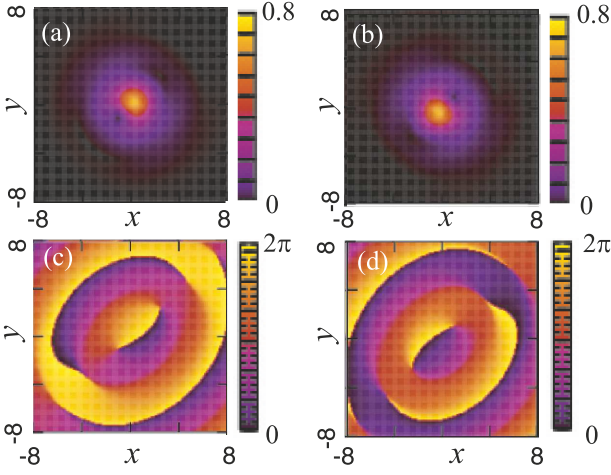


FIG. 2: Plots of (a) $|\phi_+(x, y)|$, (b) $|\phi_-(x, y)|$, (c) phase of $\phi_+(x, y)$, and (d) phase of $\phi_-(x, y)$ for a mixed-mode state at $\lambda_D = 0.05$, $\gamma = 1.1$, and $N = 3.5$.

distributions is $4\lambda_D k_x k_y$. The plots of the SV state are symmetric with respect to both diagonals $y = \pm x$, while the components of the MM state are symmetric solely with respect to $y = x$.

Figures 1(a),(b) and 2(a),(b) demonstrate that an effective size of the solitons of both the SV and MM types is $\alpha_{1,2}^{-1/2} \sim \beta_{1,2}^{-1/2} \sim 4$. Taking into regard the above-mentioned relation between the scaled and physical units, this implies that the actual size of the 2D solitons is $\sim 3 \mu\text{m}$, i.e., it is comparable to the typical length of the transverse confinement, which is a generic feature of matter-wave solitons [36].

To address in detail the crucially important effect of the switch between the SV and MM with the increase of the relative cross-attraction strength, γ , Figs. 3(a) and (b) display $|\phi_+(x, y)|$ and $|\phi_-(x, y)|$ (solid and dashed lines, respectively), as produced by the imaginary-time integration, in diagonal cross sections $y = \mp x$, for $\gamma = 0.90, 0.95, 1.00, 1.05$, and 1.10 . An essential conclusion is that the switch happens, as in the case of $\lambda_D = 0$, exactly at $\gamma = 1$, and this critical value does not depend on λ_D , as long as the 2D solitons exist.

Further, systematic simulations of the evolution of the SV and MM modes with small arbitrary perturbations added to them (not shown here in detail) demonstrate that, as well as in the case of $\lambda_D = 0$, all the existing SVs and MMs are stable, respectively, at $\gamma < 1$ and $\gamma > 1$, and unstable in the opposite case. The calculation of the

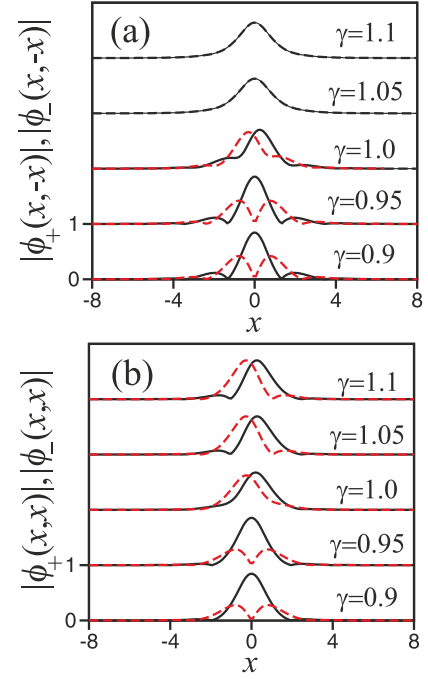


FIG. 3: (a) Profiles $|\phi_+(x, y)|$ and $|\phi_-(x, y)|$ are shown, respectively, by the solid and dashed lines in diagonal cross section $y = -x$ of the 2D solitons for $\gamma = 0.90, 0.95, 1.00, 1.05$, and 1.10 . (b) The same, shown in the perpendicular diagonal section, $y = x$. Here $\lambda_D = 0.05$ and $N = 3.5$. At $\gamma = 0.9$ and $\gamma = 1.1$ these plots correspond to Figs. 1(a),(b) and 2(a),(b), respectively.

system's energy,

$$E = \iint \left\{ \frac{1}{2} (|\nabla\phi_+|^2 + |\nabla\phi_-|^2) - \frac{1}{2} (|\phi_+|^4 + |\phi_-|^4) - \gamma |\phi_+|^2 |\phi_-|^2 + \left[\phi_+^* \left(\hat{D}^{[-1]} - i\lambda_D \hat{D}^{[+1]} \right) \phi_- - \phi_-^* \left(\hat{D}^{[+1]} + i\lambda_D \hat{D}^{[-1]} \right) \phi_+ \right] \right\} dx dy, \quad (7)$$

for both types of the solitons corroborates that, also similar to what is known in the case of $\lambda_D = 0$ [19], the relation between the corresponding energies is $E_{SV} < E_{MM}$ at $\gamma < 1$, and vice versa at $\gamma > 1$, i.e., the SV and MM, if they exist, most plausibly realize the system's GS at $\gamma < 1$ and $\gamma > 1$, respectively (not shown here in detail).

C. Mode-delocalization transition

The most essential effect caused by the addition of the Dresselhaus SOC terms is the disappearance of the self-trapped localized modes with the increase of λ_D at a

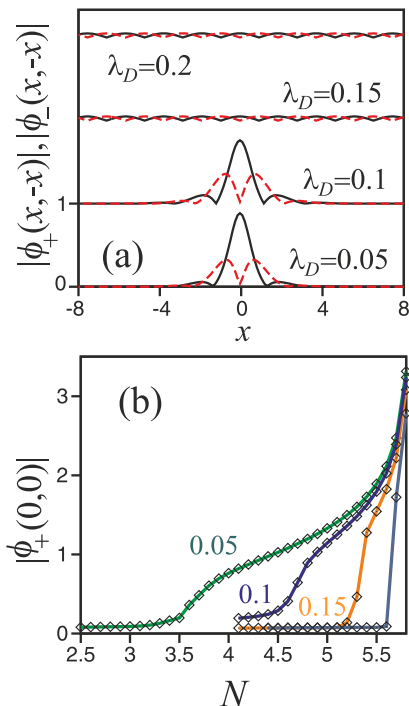


FIG. 4: (a) Fields $|\phi_+(x, y)|$ and $|\phi_-(x, y)|$ in diagonal cross section $y = -x$ at $\lambda_D = 0.05, 0.10, 0.15$, and 0.20 for $\gamma = 0$ and $N = 5$. (b) The amplitude of component $|\phi_+(x, y)|$ versus N at $\lambda_D = 0.05, 0.10, 0.15$ (marked near the plots), and 0.20 at $\gamma = 0$.

critical value, $\lambda_D^{(\text{cr})}$, followed by a transition to delocalized states at $\lambda_D > \lambda_D^{(\text{cr})}$. The growing relative strength of the Dresselhaus coupling causes the delocalization, rather than the collapse, as the norm of the solitons remains below the above-mentioned threshold necessary for the onset of the 2D wave collapse. To illustrate this effect, Fig. 4(a) displays $|\phi_+(x, y)|$ and $|\phi_-(x, y)|$ in diagonal section $y = -x$ at $\lambda_D = 0.05, 0.10, 0.15$, and 0.20 for $\gamma = 0$ and a fixed norm $N = 5$. The

SV solitons exist at $\lambda_D = 0.05$ and 0.10 , but are replaced by delocalized states already at relatively small values of the Dresselhaus-coupling strength, $\lambda_D = 0.15$ and 0.20 .

A detailed picture of the delocalization transition is provided by Fig. 4(b), which shows the amplitude (largest value) of $|\phi_+(x, y)|$ as a function of N at $\lambda_D = 0.05, 0.10, 0.15$, and 0.20 for $\gamma = 0$. The delocalization is signaled by the drop of the amplitude to very small values at $N < N_{\min}(\lambda_D)$ – for instance, with $N_{\min}(\lambda_D = 0.05) \approx 3.5$. Thus, the SV solitons exist in the interval of the norm

$$N_{\min}(\lambda_D) < N < N_{\max}(\gamma < 1), \quad (8)$$

where the largest norm,

$$N_{\max}(\gamma < 1) \approx 5.85, \quad (9)$$

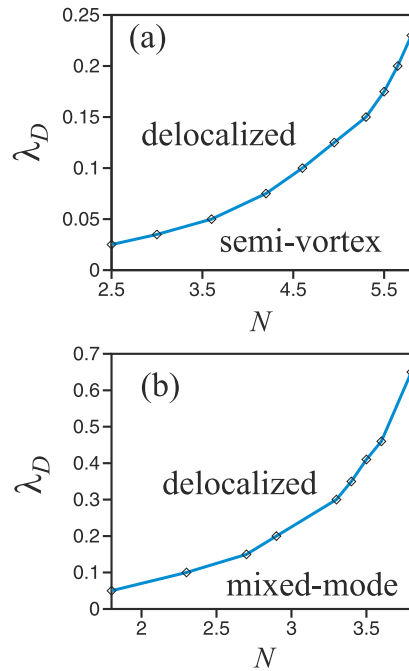


FIG. 5: Stable semi-vortex and mixed-mode solitons exist in accordingly labeled regions in the parameter plane of the norm (N) and relative strength of the Dresselhaus SOC (λ_D), in panels (a) and (b) for $\gamma = 0$ and $\gamma = 2$, respectively. The existence regions for fixed λ_D correspond to Eq. (8) at $\gamma = 0$, and to an accordingly modified interval at $\gamma = 2$, see Eq. (10).

is the critical value at which the 2D collapse commences in the framework of the NLSE in free space, hence no solitons can exist at $N > N_{\max}(\gamma < 1)$. In the limit of $N \rightarrow N_{\max}(\gamma < 1)$, which corresponds to $\mu \rightarrow -\infty$, the bimodal SV soliton degenerates into the fundamental Townes soliton in one component, with $N = N_{\max}(\gamma < 1)$ in it, while the other component becomes empty. Therefore, $N_{\max}(\gamma < 1)$ does not depend on γ in the interval of $\gamma < 1$, where the SV plays the role of the GS. According to the estimate of actual physical parameters presented above, $N_{\max} \approx 5.85$ implies that the number of atoms in the soliton is limited by $\sim 15,000$.

The results for both the SV and MM solitons are summarized by Fig. 5, which shows the regions in the (N, λ_D) planes in which the solitons exist and are stable (as has been verified by means of systematic real-time simulations of their perturbed evolution). Note that, in panel 5(b), the largest norm corresponds to the value (9) subjected to obvious rescaling,

$$N_{\max}(\gamma > 1) = \frac{2}{1 + \gamma} N_{\max}(\gamma < 1). \quad (10)$$

This is explained by the fact that, in the limit of $N \rightarrow N_{\max}(\gamma > 1)$, which again corresponds to $\mu \rightarrow -\infty$, the vortical terms vanish in ansatz (6), and the soliton degenerates into a bound state of two identical Townes solitons

in both components. It is worthy to note that the MM solitons are more immune to the destructive effect of the Dresselhaus coupling: while the SV modes exist up to $\lambda_D \approx 0.23$ in Fig. 5(a), for their MM counterparts the existence regions extends up to $\lambda_D \approx 0.65$, in Fig. 5(b).

III. EFFECT OF THE ZEEMAN SPLITTING ON 2D SOLITONS

A. The model

In this section, we focus on 2D solitons in the SOC system which includes the Rashba coupling (with scaled strength $\lambda \equiv 1$) and the Zeeman effect. The latter one breaks the symmetry between the two components of the pseudo-spinor wave function (the full Rashba-Dresselhaus coupling is also considered below, in a brief form). The corresponding scaled GPE system is

$$i\frac{\partial\phi_+}{\partial t} = -\frac{1}{2}\nabla^2\phi_+ - (|\phi_+|^2 + \gamma|\phi_-|^2)\phi_+ + \widehat{D}^{[-]} \phi_- - \Omega\phi_+, \quad (11)$$

$$i\frac{\partial\phi_-}{\partial t} = -\frac{1}{2}\nabla^2\phi_- - (|\phi_-|^2 + \gamma|\phi_+|^2)\phi_- - \widehat{D}^{[+]} \phi_+ + \Omega\phi_-, \quad (12)$$

where Ω is the strength of the Zeeman splitting, which is induced, in the BEC setting, by the optical synthetic magnetic field directed along the z -axis [4, 8, 9]. The spectrum of the linearized version of Eqs. (11), (12) is

$$\epsilon_{\pm} = \frac{k^2}{2} \pm \sqrt{k^2 + \Omega^2}, \quad (13)$$

with a gap 2Ω at $k = 0$ (cf. the gapless Rashba-Dresselhaus spectrum given by Eq. (4)). In terms of the estimate for physical parameters given above, a characteristic strength $\Omega = 1$ corresponds, in physical units, to $\sim 2\pi \times 100$ Hz for ^{85}Rb , or $2\pi \times 1$ KHz for ^7Li .

Below, we will make use of the system's energy (Hamiltonian), which now has the form

$$E = \iint \left\{ \frac{1}{2} (|\nabla\phi_+|^2 + |\nabla\phi_-|^2) - \frac{1}{2} (|\phi_+|^4 + |\phi_-|^4) - \gamma|\phi_+|^2|\phi_-|^2 - \Omega(|\phi_+|^2 - |\phi_-|^2) + [\phi_+^* \widehat{D}^{[-]} \phi_- - \phi_-^* \widehat{D}^{[+]} \phi_+] \right\} dx dy, \quad (14)$$

cf. Eq. (7). Obviously, the increase in $\Omega > 0$ should lead to transfer of atoms from the (pseudo) spin-up component, ϕ_- , to the spin-down one, ϕ_+ , thus attenuating the SOC between the components and modifying the effect of cross-interaction.

Stationary solutions of Eqs. (11), (12) for 2D solitons with real chemical potential μ are looked for as

$\phi_{\pm} = \exp(-i\mu t) u_{\pm}(x, y)$, where complex stationary wave functions are determined by equations

$$\mu u_+ = -\frac{1}{2}\nabla^2 u_+ - (|u_+|^2 + \gamma|u_-|^2)u_+ + \widehat{D}^{[-]} u_- - \Omega u_+, \quad (15)$$

$$\mu u_- = -\frac{1}{2}\nabla^2 u_- - (|u_-|^2 + \gamma|u_+|^2)u_- - \widehat{D}^{[+]} u_+ + \Omega u_-. \quad (16)$$

B. Analytical approaches: large Zeeman splitting and asymptotics of the SV wave function.

An analytical approximation can be developed in the limit of large positive Ω , when Eq. (15) demonstrates that the chemical potential is close to $-\Omega$:

$$\mu = -\Omega + \delta\mu, \quad |\delta\mu| \ll \Omega. \quad (17)$$

The spin-down component, u_- , being vanishingly small in this limit, Eq. (16) simplifies to

$$u_- \approx \frac{1}{2\Omega} \widehat{D}^{[+]} u_+, \quad (18)$$

where $(\Omega - \mu)$ is replaced by 2Ω , pursuant to Eq. (17). Then, the substitution of approximation (18) into Eq. (15) leads to the following equation for u_+ :

$$(\delta\mu) u_+ = -\frac{1}{2} \left(1 - \frac{1}{\Omega} \right) \nabla^2 u_+ - |u_+|^2 u_+. \quad (19)$$

By itself, Eq. (19) is tantamount to the NLSE in the free 2D space, which gives rise to the Townes solitons; then, Eq. (18) generates a small vortex component of the SV complex. A crucially important fact is the necessity to scale out factor $(1 - 1/\Omega)$ in Eq. (19). Due to the smallness of $1/\Omega$, the scaling easily demonstrates that the norm of the SV complex is, in the present case,

$$N = \left(1 - \frac{1}{\Omega} \right) N_{\max} (\gamma < 1) + \mathcal{O} \left(\frac{1}{\Omega^2} \right), \quad (20)$$

where the last term is a second-order correction corresponding to the norm of the small vortex component given by Eq. (18). Thus, Eq. (20) (which is compared to the corresponding numerically found dependence below in Fig. 8) demonstrates that the total norm of the SV soliton, produced by the present approximation, is (slightly) *smaller* than the collapse threshold, $N_{\max} (\gamma < 1)$. For this reason, the SV soliton remains *protected* against the collapse and stable, still realizing the GS of the system.

The approximation can be extended to the more general system, when the SOC includes both the Rashba and Dresselhaus terms, see Eqs. (2),(3). In this case, Eq. (18) is replaced by

$$u_- \approx \frac{1}{2\Omega} \widehat{D}^{[+]} u_+ + \frac{i\lambda_D}{2\Omega} \widehat{D}^{[-]} u_+, \quad (21)$$

and Eq. (19) takes a more general form too:

$$(\delta\mu)u_+ = -\frac{1}{2}\left(1 - \frac{1 + \lambda_D^2}{\Omega}\right)\nabla^2 u_+ + \frac{2\lambda_D}{\Omega}\frac{\partial^2 u_+}{\partial x \partial y} - |u_+|^2 u_+. \quad (22)$$

The transformation

$$\begin{aligned} x &\equiv \left(1 - \frac{1 + \lambda_D^2}{2\Omega}\right)\xi - \frac{\lambda_D}{\Omega}\eta, \\ y &\equiv \left(1 - \frac{1 + \lambda_D^2}{2\Omega}\right)\eta - \frac{\lambda_D}{\Omega}\xi \end{aligned} \quad (23)$$

provides for the diagonalization of the linear operator in Eq. (22), again casting it in the form of the 2D free-space NLSE, and making it possible to use the Townes soliton as a solution for u_+ , in terms of coordinates (ξ, η) . Finally, the Jacobian of transformation (23) leads to a generalization of Eq. (20),

$$N = \left(1 - \frac{1 + \lambda_D^2}{\Omega}\right)N_{\max}(\gamma < 1) + \mathcal{O}\left(\frac{1}{\Omega^2}\right). \quad (24)$$

As well as Eq. (20), this result, having $N < N_{\max}(\gamma < 1)$, secures the protection of the SV soliton against the collapse, i.e., its stability.

Note that the lowest-order approximation developed here does not give rise to terms including γ , and actually implies that, in the limit of large Ω , all solitons, if they are still stable, belong to the SV type, irrespective of the value of γ . This conclusion is consistent with more general results produced below.

In addition, one can find analytically the asymptotic form of the wave function in the presence of the Zeeman splitting. For $\Omega = 0$, an asymptotic form of the SV soliton solution to Eqs. (11), (12) at $r \rightarrow \infty$ was found in Ref. [19]:

$$\begin{aligned} \phi_+(x, y, t) &= e^{-i\mu t} f_1(r), \\ \phi_-(x, y, t) &= e^{-i\mu t + i\theta} r f_2(r), \end{aligned} \quad (25)$$

with

$$f_1^{(\Omega=0)} \approx F r^{-1/2} e^{-r/R_{SV}} \cos(r/L_{so} + \delta), \quad (26)$$

$$f_2^{(\Omega=0)} \approx -F r^{-3/2} e^{-r/R_{SV}} \sin(r/L_{so} + \delta), \quad (27)$$

where F and δ are arbitrary real constants, $R_{SV} = 1/\sqrt{-(2\mu + 1)}$ is the localization radius of the state, and $L_{so} = 1$ (in the present notation) is the spin precession length due to the spin-orbit coupling. As it follows from condition of real R_{SV} , the localized modes exist at values of the chemical potential

$$\mu < -1/2. \quad (28)$$

In the presence of a moderately strong Zeeman splitting, with $0 < \Omega < 1$, the SV solitons exist at

$$\mu < -\frac{1 + \Omega^2}{2}, \quad (29)$$

cf. existence region (17) at $\Omega = 0$. In this case, the asymptotic form of the soliton is more complex than one given by Eq. (27), with the localization and precession lengths presented as

$$R_{SV}^{-1} = \sqrt{-(\mu + 1) + \sqrt{\mu^2 - \Omega^2}}, \quad (30)$$

$$L_{so}^{-1} = \frac{\sqrt{-(2\mu + 1 + \Omega^2)}}{\sqrt{-(\mu + 1) + \sqrt{\mu^2 - \Omega^2}}}. \quad (31)$$

Strong Zeeman splitting, with $\Omega > 1$, replaces existence condition (29) by $\mu < -1$. More specifically, the SV solitons keep the asymptotic form (30) in the semi-infinite interval (29) of the chemical potentials. However, in the additional finite interval appearing in this case,

$$-\frac{1 + \Omega^2}{2} < \mu < -1, \quad (32)$$

the SV soliton exhibits a more dramatic change of its asymptotic shape: since the Zeeman coupling suppresses the displacement-dependent spin rotation, the radial oscillations vanishes, while the exponential decay of the solution at $r \rightarrow \infty$ is provided by

$$R_{SV} = \frac{1}{\sqrt{-2(\mu + 1 + \sqrt{2\mu + 1 + \Omega^2})}}. \quad (33)$$

This analytical prediction is compared to numerical results in Fig. 6(b) below.

C. Semi-vortex states

We begin with the SVs, which, as shown below, are more immune to the action of the Zeeman splitting than the MM states. First, a VA may be applied, similar to that developed for the case of $\Omega = 0$ in Ref. [19]. Using for this purpose the Gaussian ansatz (5) and substituting it into expression (14) for the system's energy yields the energy as a function of parameters of the ansatz, $A_{1,2}$ and $\alpha_{1,2}$:

$$\begin{aligned} E_{SV} &= \pi \left[\frac{A_1^2}{2} - \frac{A_1^4}{8\alpha_1} + \frac{A_2^2}{2\alpha_2} - \frac{A_2^4}{64\alpha_2^3} - \frac{\gamma A_1^2 A_2^2}{4(\alpha_1 + \alpha_2)^2} + \right. \\ &\quad \left. \Omega \left(\frac{A_2^2}{4\alpha_2^2} - \frac{A_1^2}{2\alpha_1} \right) + \frac{4A_1 A_2 \alpha_1}{(\alpha_1 + \alpha_2)^2} \right], \end{aligned} \quad (34)$$

with total norm (1) expressed as

$$N_{SV} = \frac{\pi A_1^2}{2\alpha_1} + \frac{\pi A_2^2}{4\alpha_2^2}. \quad (35)$$

Then, the VA predicts values of the four parameters for the SV soliton as a point at which energy (34) attains a minimum, subject to constraint (35).

A family of the SV solitons was produced, in parallel, by means of the imaginary-time simulations of Eqs.

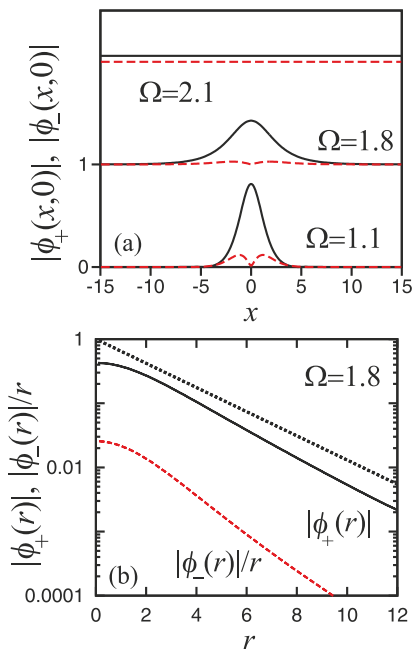


FIG. 6: (a) Profiles of $|\phi_+(x,0)|$ and $|\phi_-(x,0)|$ at $\Omega = 1.1, 1.8,$ and 2.1 for $\gamma = 0, N = 3$. (b) Profiles of $|\phi_+(r)|$ and $|\phi_-(r)|/r$ at $\Omega = 1.8$ in the log-scale. The dashed straight line is the asymptotic exponential form corresponding to Eq. (33).

(11), (12) and via the VA. Since the axial symmetry here is preserved, we use the (r, θ) as well as the (x, y) representation to describe the SV states. Figure 6(a) shows the profiles of $|\phi_+(r)|$ and $|\phi_-(r)|$ at $\Omega = 1.1, 1.8,$ and 2.1 for $\gamma = 0, N = 3$. For $\Omega = 1.8, \mu$ satisfies the condition $-(1/2)(1+\Omega^2) < \mu < -1$. Figure 6(b) compares the profile of $|\phi_+(r)|$ with the asymptotic form in Eq. (33). The result is that, at a fixed value of N , the soliton's amplitude decreases, while the soliton spreads out, with the increase in Ω . Eventually, the amplitude vanishes at some critical field, $\Omega = \Omega_{\text{cr}}$, and only delocalized states exist after this threshold. Figures 7(a) and (b) display this trend by showing the amplitudes of (a) the larger (spin-up) component, $|\phi_+(r)|$, and (b) the smaller (spin-down) component, $|\phi_-(r)|$, as a function of Ω for $\gamma = 0$ and a fixed norm $N = 3$. In this case, the delocalization sets in at

$$\Omega_{\text{cr}}(N = 3) \approx 1.95. \quad (36)$$

It is also seen that the VA provides a reasonable accuracy, predicting, in particular, $\Omega_{\text{cr}}^{(\text{VA})}(N = 3) \approx 1.83$, with relative error $\approx 6\%$.

Figure 8 produces a summary of the numerical and variational results for the SV solitons, showing the existence region for stable SVs in the parameter plane of (N, Ω) for $\gamma = 0$. Although the plot is confined to $N \leq 5.25$, the analytical result given above by Eqs. (18)-(20) suggests that the SV existence boundary in Fig. 8(b)

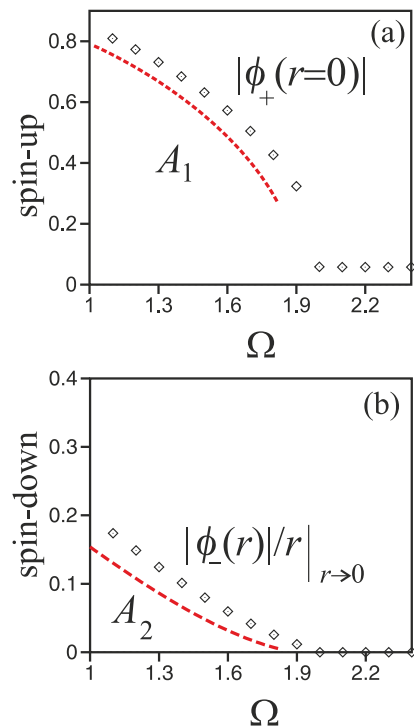


FIG. 7: (a) The amplitude of the larger (spin-up) component, $|\phi_+(r)|$, in the SV state as a function of strength Ω of the Zeeman splitting, for $\gamma = 0$ and $N = 3$. (b) The amplitude of the smaller (spin-down) component, $|\phi_-(r)|$, as a function of strength Ω of the Zeeman splitting, for $\gamma = 0$ and $N = 3$. In both panels (a) and (b), chains of rhombuses and dashed lines show, severally, numerical results and their counterparts produced by the variational approximation based on the minimization of energy (34), subject to constraint (35).

extends to $\Omega \rightarrow \infty$ in the limit of $N \rightarrow N_{\text{max}}(\gamma < 1) \approx 5.85$.

D. Mixed-mode states and mixed-mode - semi-vortex transitions

As well as in the case of the SVs, the increase of strength Ω of the Zeeman splitting leads to the reduction of the amplitude of the spin-down component ϕ_- of the MM soliton, in comparison with its spin-up counterpart, ϕ_+ , as shown in Fig. 9. However, it is also observed in Fig. 9 that, instead of the delocalization, the MM undergoes a transformation into a stable SV soliton – even at $\gamma > 1$, when solely the MM states, but not SVs, may be stable in the absence of the Zeeman splitting.

Thus, it is relevant to identify the shift of the MM-SV conversion from point $\gamma = 1$, which was the universal boundary between the SV and MM shapes of the GS at $\Omega = 0$, to $\gamma > 1$. This important characteristic of the system can be predicted by means of the VA, using ansatz (6) as an approximation for the MM state. The substitution of the ansatz into Eqs. (14) and (1) yields

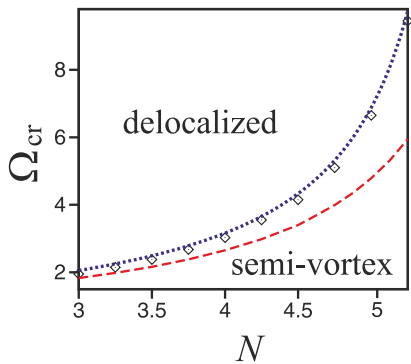


FIG. 8: The critical value Ω_{cr} , up to which the semi-vortex soliton persists, versus its norm N , for $\gamma = 0$. Chains of rhombuses and dashed lines show, correspondingly, numerical results and their counterparts produced by the variational approximation based on the minimization of energy. The dotted line is the prediction of Eq. (20).

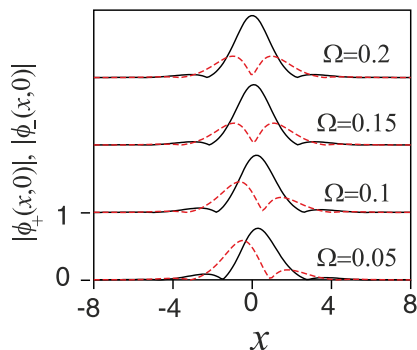


FIG. 9: Profiles of the spin-up and spin-down components, $|\phi_+(x,0)|$ and $|\phi_-(x,0)|$ (shown by continuous and dashed lines, respectively) of mixed-mode solitons at the Zeeman splitting $\Omega = 0.05, 0.10, 0.15$, and 0.20 , for $\gamma = 1.5$ and $N = 3$. Eventually, the mixed mode transforms into a semi-vortex.

the following expressions, cf. Eqs. (34) and (35):

$$E_{\text{MM}} = \pi \left[B_1^2 + \frac{B_2^2}{\beta_2} - (1 + \gamma) \left(\frac{B_1^4}{4\beta_1} + \frac{B_2^4}{32\beta_2^3} \right) - \frac{B_1^2 B_2^2}{(\beta_1 + \beta_2)^2} + \frac{8B_1 B_2 \beta_1}{(\beta_1 + \beta_2)^2} \right], \quad (37)$$

$$N = \frac{\pi B_1^2}{\beta_1} + \frac{\pi B_2^2}{2\beta_2^2}. \quad (38)$$

Then, parameters of the MM solitons are predicted by the present version of the VA as those at which energy (37) attains a minimum, subject to the constraint of keeping the fixed norm, as per Eq. (38). Note, in particular, that this approximation for the energy, produced by ansatz (6), does not contain Ω (in contrast with its SV counterpart (34)) because ansatz (6) implies equal norms of ϕ_+

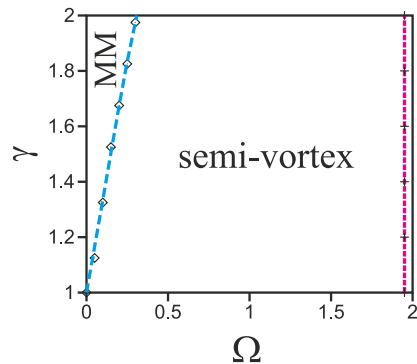


FIG. 10: The chain of rhombuses shows the numerically found cross-attraction strength, γ , at which the ground state switches from the mixed mode to the semi-vortex, as a function of the Zeeman Ω for the norm $N = 3$. The dashed line is the same dependence as predicted by the variational approximation, see Eq. (40). The ground state is the semi-vortex beneath this line, and the mixed mode above it. The vertical line at $\Omega \approx 1.95$ is the Zeeman coupling at which the semi-vortex with $N = 3$ suffers the delocalization, see Eq. (36).

and ϕ_- , hence the respective expectation value, which determines the Zeeman energy, vanishes:

$$\langle \sigma_z \rangle = \frac{1}{N} \iint (|\phi_+|^2 - |\phi_-|^2) dx dy = 0. \quad (39)$$

This circumstance suggests that the SV state may provide lower energy in the presence of the Zeeman splitting, thus realizing the GS even at $\gamma > 1$.

The VA predicts the transition from the MM to SV as a point at which the minima of energies predicted by Eqs. (34) and (37) become equal, for a given norm,

$$\min \{E_{\text{MM}}(N)\} = \min \{E_{\text{SV}}(N)\}. \quad (40)$$

The result, in the form of the $\gamma(\Omega)$ dependence following from Eq. (40), along with its numerically generated counterpart, is displayed in Fig. 10, which demonstrates that the VA provides for a very accurate prediction of the MM \rightarrow SV transition point.

The vertical dashed line in Fig. 10, which bounds the existence area of the SVs, corresponds to the critical value of Ω , given by Eq. (36), at which the SV with norm $N = 3$ suffers delocalization. Although this Ω_{cr} was obtained above for $\gamma = 0$, it actually pertains to all values of γ , because, as seen from Fig. 7, close to the delocalization transition, the amplitude of the ϕ_- component becomes negligibly small in comparison with that of ϕ_+ , hence the cross-interaction term is also negligible at the delocalization point, in comparison with its self-interaction counterpart.

IV. CONCLUSION

In this paper, we have extended the analysis for 2D solitons in the pseudo-spinor BEC with attractive non-linearity, which may be stabilized in the form of SV (semi-vortex) and MM (mixed-mode) localized states by the SOC (spin-orbit coupling). We have considered the generic case of the combined Rashba-Dresselhaus SOC and analyzed the effect of the Zeeman splitting in the presence of the Rashba coupling. Families of SV and MM solitons have been constructed by means of numerical and approximate analytical methods, the largest number of atoms possible in the solitons under physically relevant conditions being $\sim 1.5 \times 10^4$, while as characteristic size of the solitons is $\sim 3 \mu\text{m}$. The increase in the strength of the Dresselhaus coupling preserves the soliton type (SV or MM) and eventually leads its delocalization. The sufficiently strong Zeeman splitting converts the MM solitons into the SV ones, which also eventually suffer delocalization. The existence regions have been found for both soliton species. These results help to understand novel possibilities for the creation of stable vorticity-bearing solitons in matter-wave settings, offered by the introduc-

tion of the SOC in its generic form and the synthetic Zeeman splitting.

As an extension of the present analysis, it may be interesting to consider mobility of the stable solitons in the present system with broken Galilean invariance. A challenging possibility is to study effects of the Zeeman splitting on metastable 3D SOC-supported solitons which were recently found in Ref. [31]. More generally speaking, the present results may find their application for the stabilization of 2D solitons in other nonlinear models.

Acknowledgments

B.A.M. appreciates hospitality of the Interdisciplinary Graduate School of Engineering Sciences at the Kyushu University (Fukuoka, Japan), and of Department of Physical Chemistry of the University of the Basque Country. E.Y.S. acknowledges support of the University of the Basque Country UPV/EHU under program UFI 11/55, Spanish MEC (FIS2012-36673-C03-01 and FIS2015-67161-P), and Grupos Consolidados UPV/EHU del Gobierno Vasco (IT-472-10).

-
- [1] W. Ketterle, Rev. Mod. Phys. **74**, 1131 (2002).
- [2] L. P. Pitaevskii and S. Stringari, *Bose-Einstein Condensation*, Oxford University Press (Oxford, 2003); H. T. C. Stoof, K. B. Gubbels, and D. B. M. Dickerheid, *Ultracold Quantum Fields* (Springer: Dordrecht, 2009).
- [3] S. L. Cornish, N. R. Claussen, J. L. Roberts, E. A. Cornell, and C. E. Wieman, Phys. Rev. Lett. **85**, 1795 (2000); G. Roati, M. Zaccanti, C. D'Errico, J. Catani, M. Modugno, A. Simoni, M. Inguscio, and G. Modugno, *ibid.* **99**, 010403 (2007); S. E. Pollack, D. Dries, M. Junker, Y. P. Chen, T. A. Corcovilos, and R. G. Hulet, *ibid.* **102**, 090402 (2009); D. J. Papoular, G. V. Shlyapnikov, and J. Dalibard, Phys. Rev. A **81**, 041603(R) (2010); T. V. Tscherbul, T. Calarco, I. Lesanovsky, R. V. Krems, A. Dalgarno, and J. Schmiedmayer, *ibid.* **81**, 050701(R) (2010); S. Tojo, Y. Taguchi, Y. Masuyama, T. Hayashi, H. Saito, and T. Hirano, *ibid.* **82**, 033609 (2010); R. Yamazaki, S. Taie, S. Sugawa, and Y. Takahashi, Phys. Rev. Lett. **105**, 050405 (2010); M. Yan, B. J. DeSalvo, B. Ramachandhran, H. Pu, and T. C. Killian, *ibid.* **110**, 123201 (2013); L. W. Clark, L.-C. Ha, C.-Y. Xu, and C. Chin, *ibid.* **115**, 155301 (2015); M. Höfer, L. Riegger, F. Scazza, C. Hofrichter, D. R. Fernandes, M. M. Parish, J. Levinsen, I. Bloch, and S. Fölling, *ibid.* **115**, 265302 (2015).
- [4] Y. J. Lin, K. Jimenez-Garcia, and I. B. Spielman, Nature **471**, 83 (2011); J.-Y. Zhang, S.-C. Ji, Z. Chen, L. Zhang, Z.-D. Du, B. Yan, G.-S. Pan, B. Zhao, Y. J. Deng, H. Zhai, S. Chen, and J.-W. Pan, Phys. Rev. Lett. **109**, 115301 (2012); L. W. Cheuk, A. T. Sommer, Z. Hadzibabic, T. Yefsah, W. S. Bakr, and M. W. Zwierlein, *ibid.* **109**, 095302 (2012); C. Hamner, C. Qu, Y. Zhang, J. Chang, M. Gong, C. Zhang, and P. Engels, Nature Commun. **5**, 4023 (2014); A. J. Olson, S.-J. Wang, R. J. Niffenegger, C.-H. Li, C. H. Greene, and Y. P. Chen, Phys. Rev. A **90**, 013616 (2014).
- [5] G. Dresselhaus, Phys. Rev. **100**, 580 (1955).
- [6] Y. A. Bychkov and E. I. Rashba, J. Phys. C **17**, 6039 (1984).
- [7] D. L. Campbell, G. Juzeliūnas, and I. B. Spielman, Phys. Rev. A **84**, 025602 (2011).
- [8] H. Zhai, Int. J. Mod. Phys. B **26**, 1230001 (2012).
- [9] J. Dalibard, F. Gerbier, G. Juzeliūnas, and P. Öhberg, Rev. Mod. Phys. **83**, 1523 (2011); I. B. Spielman, in: Ann. Rev. Cold At. Mol. **1**, 145 (2012); V. Galitski and I. B. Spielman, Nature **494**, 49 (2013); X. Zhou, Y. Li, Z. Cai, and C. Wu, J. Phys. B: At. Mol. Opt. Phys. **46**, 134001 (2013); N. Goldman, G. Juzeliūnas, P. Öhberg, and I. B. Spielman, Rep. Progr. Phys. **77**, 126401 (2014).
- [10] Z. Wu, L. Zhang, W. Sun, X.-T. Xu, B.-Z. Wang, S.-C. Ji, Y. Deng, S. Chen, X.-J. Liu, and J.-W. Pan, arXiv:1511.08170.
- [11] L. Huang, Z. Meng, P. Wang, P. Peng, S.-L. Zhang, L. Chen, D. Li, Q. Zhou, and J. Zhang, Nature Physics, doi:10.1038/nphys3672.
- [12] V. Achilleos, D. J. Frantzeskakis, P. G. Kevrekidis, and D. E. Pelinovsky, Phys. Rev. Lett. **110**, 264101 (2013); Y. V. Kartashov, V. V. Konotop, and F. Kh. Abdullaev, *ibid.* **111**, 060402 (2013); Y. Xu, Y. Zhang, and B. Wu, Phys. Rev. A **87**, 013614 (2013); L. Salasnich and B. A. Malomed, *ibid.* **87**, 063625 (2013); P. Belićević, G. Gligorić, J. Petrović, A. Maluckov, L. Hadzievski, and B. Malomed, J. Phys. B At. Mol. Opt. Phys. **48**, 065301 (2015).
- [13] V. E. Lobanov, Y. V. Kartashov, and V. V. Konotop, Phys. Rev. Lett. **112**, 180403 (2014).
- [14] C. Wang, C. Gao, C.-M. Jian, and H. Zhai, Phys. Rev. Lett. **105**, 160403 (2010); D. A. Zezyulin, R. Driben,

- V. V. Konotop, and B. A. Malomed, Phys. Rev. A **88**, 013607 (2013).
- [15] T. D. Stanescu, V. Galitski, J. Y. Vaishnav, Ch. W. Clark, and S. Das Sarma, Phys. Rev. A **79**, 053639 (2009); C. J. Wu, Mod. Phys. Lett. B **23**, 1 (2009); J. Radić, T. A. Sedrakyan, I. B. Spielman, and V. Galitski, Phys. Rev. A **84**, 063604 (2011); X.-F. Zhou, J. Zhou, and C. Wu, *ibid.* **84**, 063624 (2011); Z. F. Xu, Y. Kawaguchi, L. You, and M. Ueda, *ibid.* **86**, 033628 (2012); Y. Li, L. P. Pitaevskii, and S. Stringari, Phys. Rev. Lett. **108**, 225301 (2012).
- [16] R. Feynman, *Statistical Mechanics: A Set of Lectures*, Westview Press (Boulder, 1998).
- [17] A. L. Fetter, Rev. Mod. Phys. **81**, 647 (2009).
- [18] S. Sinha, R. Nath, and L. Santos, Phys. Rev. Lett. **107**, 270401 (2011); C. J. Wu, I. Mondragon-Shem, and X.-F. Zhou, Chin. Phys. Lett. **28**, 097102 (2011); Y. Deng, J. Cheng, H. Jing, C. P. Sun, and S. Yi, Phys. Rev. Lett. **108**, 125301 (2012); T. Kawakami, T. Mizushima, and K. Machida, Phys. Rev. A **84**, 011607 (2011); B. Ramachandhran, B. Opanchuk, X.-J. Liu, H. Pu, P. D. Drummond, and H. Hu, *ibid.* **85**, 023606 (2012); G. J. Conduit, *ibid.* **86**, 021605(R) (2012); E. Ruokokoski, J. A. M. Huhtamaki, and M. Mottonen, *ibid.* **86**, 051607 (2012); H. Sakaguchi and B. Li, Phys. Rev. A **87**, 015602 (2013); A. Fetter, *ibid.* **89**, 023629 (2014); J. Low Temp. Phys. **180**, 37 (2015).
- [19] H. Sakaguchi, B. Li, and B. A. Malomed, Phys. Rev. E **89**, 032920 (2014).
- [20] T. Ozawa and G. Baym, Phys. Rev. Lett. **109**, 025301 (2012); R. Barnett, S. Powell, T. Graß, M. Lewenstein, and S. Das Sarma, Phys. Rev. A **85**, 023615 (2012).
- [21] X.-Q. Xu and J. H. Han, Phys. Rev. Lett. **107**, 200401 (2011); T. Kawakami, T. Mizushima, M. Nitta, and K. Machida, *ibid.* **109**, 015301 (2012); C.-F. Liu and W. M. Liu, Phys. Rev. A **86**, 033602 (2012); X. F. Zhou, Y. Li, Z. Cai, and C. J. Wu, J. Phys. B **46**, 134001 (2013).
- [22] L. Bergé, Phys. Rep. **303**, 259 (1998); E. A. Kuznetsov and F. Dias, *ibid.* **507**, 43 (2011); C. Sulem and P. L. Sulem, *The nonlinear Schrödinger equation: self-focusing and wave collapse* (Springer: Berlin, 1999).
- [23] B. A. Malomed, D. Mihalache, F. Wise, and L. Torner, J. Optics B: Quant. Semicl. Opt. **7**, R53 (2005).
- [24] R. Y. Chiao, E. Garmire, and C. H. Townes, Phys. Rev. Lett. **13**, 479 (1964).
- [25] V. I. Kruglov, Yu. A. Logvin, and V. M. Volkov, J. Mod. Opt. **39**, 2277 (1992).
- [26] H. Sakaguchi and B. A. Malomed, Phys. Rev. E **90**, 062922 (2014).
- [27] L. Salasnich, W. B. Cardoso, and B. A. Malomed, Phys. Rev. A **90**, 033629 (2014).
- [28] T. Ozawa and G. Baym, Phys. Rev. A **85**, 013612 (2012).
- [29] Sh. Mardonov, E. Ya. Sherman, J. G. Muga, H.-W. Wang, Y. Ban, and X. Chen, Phys. Rev. A **91**, 043604 (2015).
- [30] Y. V. Kartashov, B. A. Malomed, V. V. Konotop, V. E. Lobanov, and L. Torner, Opt. Lett. **40**, 1045 (2015).
- [31] Y.-C. Zhang, Z.-W. Zhou, B. A. Malomed, and H. Pu, Phys. Rev. Lett. **115**, 253902 (2015).
- [32] Y. Zhang, L. Mao, and C. Zhang, Phys. Rev. Lett. **108**, 035302 (2012); Y. Li, L. P. Pitaevskii, and S. Stringari, *ibid.* **108**, 225301 (2012).
- [33] S. S. Natu, X. Li, and W. S. Cole, Phys. Rev. A **91**, 023608 (2015).
- [34] The limit case of the model based on Eqs. (2) and (3) corresponding to $\lambda \rightarrow \infty$, when the second-derivative terms are negligible, amounts to an “ultrarelativistic” system, that can be studied by means of the technique developed in: L.H. Haddad and L.D. Carr, New Journ. of Phys. **17**, 063034 (2015); L.H. Haddad, C.M. Weaver, and L.D. Carr, *ibid.* **17**, 063033 (2015); L.H. Haddad and L.D. Carr, *ibid.* **17**, 093037 (2015); L.H. Haddad and L.D. Carr, *ibid.* **17**, 113011 (2015). However, in our analysis the usual kinetic energy, represented by the second derivatives, is essential.
- [35] E. Tiesinga and P. R. Johnson, Phys. Rev. A **87**, 013423 (2013); P.-S. He, W.-L. You, and W.-M. Liu, *ibid.* **87**, 063603 (2013).
- [36] K. E. Strecker G. B. Partridge, A. G. Truscott, and R. G. Hulet, Nature **417**, 150 (2002); L. Khaykovich, F. Schreck, G. Ferrari, T. Bourdel, J. Cubizolles, L. D. Carr, Y. Castin, and C. Salomon, Science **296**, 1290 (2002); K. E. Strecker, G. B. Partridge, A. G. Truscott, and R. G. Hulet New J. Phys. **5**, 73.1 (2003); S. L. Cornish, S. T. Thompson, and C. E. Wieman, Phys. Rev. Lett. **96**, 170401 (2006); A. L. Marchant, T. P. Billam, T. P. Wiles, M. M. H. Yu, S. A. Gardiner, and S. L. Cornish, Nat. Commun. **4**, 1865 (2013); P. Medley, M. A. Minar, N. C. Cizek, D. Berryrieser, and M. A. Kasevich, Phys. Rev. Lett. **112**, 060401 (2014).